PAPER

Swimming in a crystal†

Aidan T. Brown,*[a] Ioana D. Vladescu,[a] Angela Dawson,[a] Teun Vissers,[a] Jana Schwarz-Linek,[a] Juho S. Lintuvuori[ab] and Wilson C. K. Poon[a]

We study catalytic Janus particles and *Escherichia coli* bacteria swimming in a two-dimensional colloidal crystal. The Janus particles orbit individual colloids and hop between colloids stochastically, with a hopping rate that varies inversely with fuel (hydrogen peroxide) concentration. At high fuel concentration, these orbits are stable for 100s of revolutions, and the orbital speed oscillates periodically as a result of hydrodynamic, and possibly also phoretic, interactions between the swimmer and the six neighbouring colloids. Motile *E. coli* bacteria behave very differently in the same colloidal crystal: their circular orbits on plain glass are rectified into long, straight runs, because the bacteria are unable to turn corners inside the crystal.

1 Introduction

Non-equilibrium systems pose a grand challenge cutting across many areas of physics. An exciting frontier concerns microscopic swimmers, both motile micro-organisms such as bacteria and algae, and, increasingly, a range of synthetic self-propelled colloids.[1,2] Such swimmers attract interest in terms of their propulsive mechanisms[2–8] and their collective behaviour.[9] These aspects are coupled: the collective behaviour depends on how swimmers interact, and aspects of these interactions are directly related to the propulsive mechanism.

Microswimmers interact with each other and with their surroundings via two classes of interactions. Various thermodynamic interactions (van der Waals, electrostatic,...) are shared with passive particles. Their effect, at least on quiescent passive particles, can be treated using equilibrium statistical mechanics. A second class of interactions arises directly from self propulsion, and is responsible for the above-mentioned coupling between the propulsive mechanism and collective behaviour. There is as yet no general theory to predict the effect of these detailed-balance-violating interactions.

The most basic type of active interaction between self-propelled particles arises simply because of persistence in the direction of motion. This explains the ubiquitous observation that microswimmers accumulate at confining boundaries: once a swimmer reaches a wall, it takes finite time to reorient and swim away.[10] When many microswimmers are present, this interaction can induce phase separation[11,12] and collective motion.[13] Another ubiquitous active interaction arises from the flow fields responsible for self propulsion. Such hydrodynamic interactions (HI) can produce qualitatively different behaviour from persistence-induced interactions.[9,14] Indeed, phase separation driven by the latter may be suppressed by HI.[15]

Considering persistence-induced interactions and HI often suffices for understanding biological microswimmers, because the metabolic reactions powering self propulsion[16] are typically internal. Other, specific interactions such as quorum sensing are not integral to the propulsion, and can generally be switched off genetically. By contrast, synthetic active colloids often swim via self-generated external gradients, *e.g.* of electrostatic potential, chemical concentration or temperature. So-called phoretic interactions (PI)[17–21] can arise from the coupling of these gradients to other surfaces and swimmers. Since these external gradients are by definition strong enough to generate the flow-fields required to propel the particle, the interactions produced by these gradients can be expected to also have comparable magnitude to the HI.

Active interactions can be accessed experimentally by directly studying swimmer-swimmer interactions in dilute suspensions,[22] and also by looking at the interactions between swimmers and passive tracer particles,[23–25] surfaces[18,26–31] or porous media.[10,32] In this article, we focus on the interaction between swimmers and a model porous medium. We observe two popular swimmers, catalytic Pt–polystyrene Janus particles[5] and *Escherichia coli* bacteria,[16] interacting with a close-packed 2D crystal of passive colloids.

This environment has opposite effects on these two swimmers: it destroys the usual orbital motion of *E. coli* on plane surfaces,[33–35]

[a] *SUPA, School of Physics and Astronomy, The University of Edinburgh, King's Buildings, Peter Guthrie Tait Road, Edinburgh, EH9 3FD, UK. E-mail: abrown20@staffmail.ed.ac.uk*

[b] *Laboratoire de Physique des Solides, Université Paris-Sud, UMR 8502-91405 Orsay, France*

† Electronic supplementary information (ESI) available: See Appendix A for captions to Videos S1–S4. Data on which this article are based are accessible online through Edinburgh DataShare (DOI: 10.7488/DS/304). See DOI: 10.1039/c5sm01831e

but induces orbital motion of the Janus swimmers around individual colloids in the crystal. We can explain the behaviour of *E. coli* cells simply, in terms of the steric hindrance between their long flagella bundles and their crystalline surroundings. Orbiting Janus swimmers are harder to understand. They hop stochastically between orbits round neighbouring colloids. The hopping rate scales inversely with the concentration of the fuel, H_2O_2, but is independent of the speed of the swimmers at a particular fuel concentration. This suggests that orbital trapping is not just a hydrodynamic effect, but also involves PI. While there is insufficient information to pin down a specific trapping mechanism, we have characterised the trapping empirically in terms of a stiffness and an effective potential, which should help constrain future theory construction.

We observed extremely long-lived orbits at high H_2O_2 concentrations, lasting for 100s of rotations (10s of minutes). These could form the basis for useful devices – most obviously, a microfluidic stirrer,[32] and for studying the complex interactions between multiple orbiting swimmers.[36]

Finally, we find that the orbital speed oscillates, resulting from interactions between the orbiting swimmer and the six colloids neighbouring the orbit. These oscillations contain information on the propulsion mechanism, which dictates the character of the active interactions. However, current, incomplete understanding of the phoretic propulsion of Janus swimmers[7,8] means that we cannot unambiguously disentangle the contributions of HI and PI to the observed speed oscillations. We therefore discuss our results in terms of a simple model swimmer interacting purely via HI with its surroundings. With future advances in the understanding of PI in catalytic swimmers, our results should help constrain proposals for their propulsion mechanism.

2 Janus swimmers

2.1 Materials and methods

We prepared Janus particles (5 nm Pt sputtered on 2 μm diameter fluorescent polystyrene colloids from Invitrogen[7]) and suspended them in aqueous H_2O_2 (Acros) solutions at volume fraction $\sim 10^{-6}$ v/v. We placed this suspension in chambers formed between glass slides (Menzel) and 22×22 mm^2 glass coverslips (Bettering) with 300 μm thick parafilm spacers.

On the coverslips, close-packed 2D colloidal crystals had been formed beforehand by depositing 10 μm diameter polystyrene colloids (Thermo-Fisher) at 1% v/v in water and evaporating at 70 °C. The radii of the static colloids, $R = 5.06 \pm 0.02$ μm, and Janus swimmers, $a = 0.96 \pm 0.04$ μm, were determined by repeated ($25\times$) measurement of interparticle distances in close-packed 2D crystals.

The Janus particles are bottom-heavy,[7,37] and therefore swim upwards. In addition, they will swim stably along a surface irrespective of its orientation.[7,37] Hence, to collect the swimmers in the colloidal crystal, we initially oriented the chamber with the coated coverslip uppermost, allowing the swimmers to collect there, before inverting the chamber for observation with an
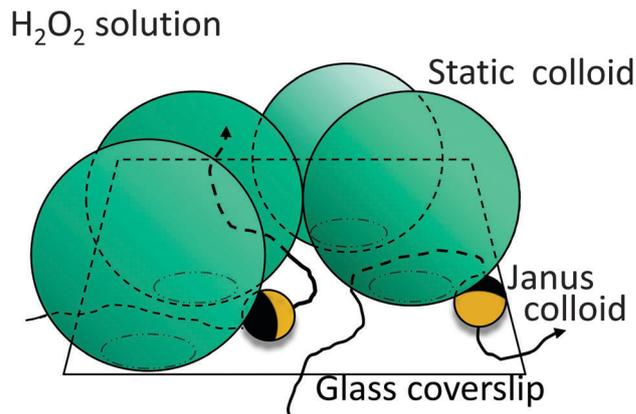

Fig. 1 Schematic of the experimental setup.

inverted epifluorescence microscope (Ti Eclipse, Nikon, $\times 20$ objective) with a CCD camera (Eosens, Mikrotron). We checked that this inversion left the swimmer behaviour unchanged. On colliding with a colloid at the edge of the crystal, the swimmers orbit that colloid in the wedge-like space between colloid and coverslip (Fig. 1) before hopping out of the crystal or into orbit around another colloid.

We varied the concentration of H_2O_2 between 0.1 and 10% v/v, and tracked the swimmers (using MATLAB[7,38]) to determine the mean hopping rate and the swimming speed inside and outside the crystal at each H_2O_2 concentration. We also measured at high magnification (using a $100\times$ objective) the temporal variation in the speed of swimmers in 10% H_2O_2.

2.2 Orbital trapping

At all H_2O_2 concentrations, Janus particles orbit colloids within the crystal, and hop between neighbouring orbits. However, the residence time of a Janus particle in a particular orbit varied widely with the H_2O_2 concentration. Fig. 2a shows typical trajectories of Janus swimmers in colloidal crystals in 1% and 10% H_2O_2. In 1% H_2O_2, swimmers hop rapidly through the crystal (ESI,† Video S1), whereas in 10% H_2O_2, the hopping rate is much reduced, so that the swimmers remain in orbit around a single colloid for many minutes. Quantitatively, Fig. 2b shows this hopping rate, Γ, as a function of H_2O_2 concentration ($[H_2O_2]$). The solid line is a fit to $\Gamma \propto [H_2O_2]^{-1}$.
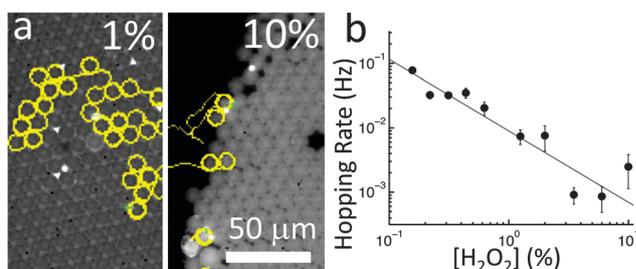

Fig. 2 Orbital hopping behaviour of Janus swimmers. (a) Tracked video of Janus swimmers inside colloidal crystals with 1% and 10% H_2O_2, each of 3 min duration. (b) Hopping rate *vs.* H_2O_2 concentration, $[H_2O_2]$. Solid line: $\Gamma \propto [H_2O_2]^{-1}$.

We will now try to understand the trapping mechanism. We first assess the possibility that the orbiting is due to passive interactions alone. The distance between the swimmer and the colloid surface is of order 100 nm (see Appendix B for details), which excludes short-ranged passive interactions such as dispersion forces. Electrostatic interactions do have sufficient range, but all our colloidal surfaces (see Appendix C) and the glass[39,40] are negatively charged, so electrostatic interactions should not result in trapping. Gravity can also be ruled out, as orbiting is observed even if the crystal is inverted or on a vertical surface (see Appendix B).

We therefore turn to active interactions. It has been suggested[32] that the orbital trapping in the related system of Pt–Au nanorods is purely hydrodynamic. In trapping by pure HI, the hopping rate Γ would be determined by a balance between HI, which maintain a stable swimmer orientation and position, and thermal fluctuations, which disrupt this stability.[32] HI increase with swimming speed, so pure hydrodynamic trapping should result in a strong negative correlation between swimming speed and hopping rate.

As shown in Fig. 3a, at all H_2O_2 concentrations, the mean speed $\langle u_c \rangle$ inside the crystal is larger than that on plain glass, $\langle u_g \rangle$. The speed saturates at high H_2O_2 concentration, as previously observed.[5] This has been attributed to the saturation of Pt binding sites by H_2O_2 molecules, which gives a predicted speed of the form[5]

$$\langle u \rangle = \frac{u^*[H_2O_2]}{[H_2O_2]^* + [H_2O_2]},\qquad(1)$$

where u^* is the saturation speed, and $[H_2O_2]^*$ is the H_2O_2 concentration at half maximum. The solid and dashed lines in Fig. 3a are best fits to eqn (1) with $u_g^* = 6.6 \pm 1\ \mu\mathrm{m\ s}^{-1}$ and $u_c^* = 11.1 \pm 2\ \mu\mathrm{m\ s}^{-1}$, and $[H_2O_2]_c^* = 0.22\% \pm 0.1\%$ and $[H_2O_2]_g^* = 0.27\% \pm 0.1\%$.

However, at each H_2O_2 concentration, there is also a wide variation in the swimming speed of individual Janus particles, probably due to variations in the Pt coating. In Fig. 3b, we therefore plot the hopping rate Γ of individual swimmers versus their orbital swimming speed. In contrast to the expectation of a purely hydrodynamic trapping model, we see no systematic variation of Γ with swimming speed, i.e. the coloured curves corresponding to individual H_2O_2 concentrations are all much flatter than the black curve through the mean speeds and hopping rates. Hence, the trapping is strongly dependent on H_2O_2 concentration, but via some speed-independent mechanism.

Apart from pure hydrodynamics, other active trapping mechanisms have been proposed, such as combinations of hydrodynamics with either short-ranged repulsive electrostatics[41] or phoretic interactions.[18] However, it is difficult to make firm conclusions because of continuing uncertainty over the propulsion mechanism, which will have a critical effect on the nature and strength of the hydrodynamic and phoretic fields. While there is strong evidence against the originally-proposed self-diffusiophoretic mechanism,[7] the details of the true mechanism, which appears to be some version of self-electrophoresis, remain obscure.[7,8] Nevertheless, the observed $\Gamma \propto [H_2O_2]^{-1}$ dependence should provide a strong constraint for future theories of the propulsion and interaction mechanisms of these swimmers.
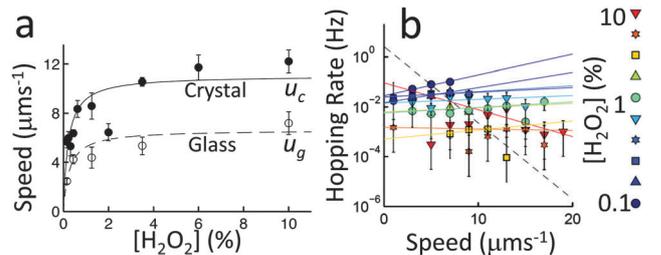
Fig. 3 The effect of propulsion speed on hopping rate. (a) Mean ballistic speed u inside (u_c, ●), and outside (u_g, ○) crystal. Solid and dashed lines are fits to eqn (1). (b) Hopping rate binned by speed for each $[H_2O_2]$ (colour-coded). Solid lines: exponential fits within each $[H_2O_2]$; dashed line: exponential fit through the mean of each data set.

Even in ignorance of the trapping mechanism, we can still attempt to quantify the trapping strength. Our stable orbit corresponds to a fixed point in a 4-dimensional phase space (two orientational and two translational degrees of freedom, assuming that the swimmer is axisymmetric and that we can ignore the relatively small interactions with neighbouring colloids, see below). Assuming that there are no limit cycles near this fixed point, we can treat the swimmer as though it were trapped in a potential well in this 4-dimensional space.[53] For two of these parameters, the horizontal angle β between the swimmer axis and the tangent to the orbit, and the radius ρ of the orbit (see Fig. 4 for definitions, and Appendix B for measurement details), we measured the temporal standard deviations, $\sigma_\beta = 1.9°$ and $\sigma_\rho = 12$ nm. Using the equipartition theorem, we then obtain the stiffness of the trapping potential in each of these directions: $k_\beta = k_B T/\sigma_\beta^2 = 4 \times 10^{-18}$ J, and $k_\rho = k_B T/\sigma_\rho^2 = 3 \times 10^{-5}$ J m^{-2}.

Similarly, from the hopping rate, Γ, we can estimate the depth of the effective trapping potential U using the Kramers theory of escape over a potential barrier, which predicts an escape frequency[42]

$$\Gamma \approx A \exp\left(-\frac{U}{k_B T}\right).\qquad(2)$$

The attempt rate A depends on the form of the potential, which is unknown; but A typically has the form[42]

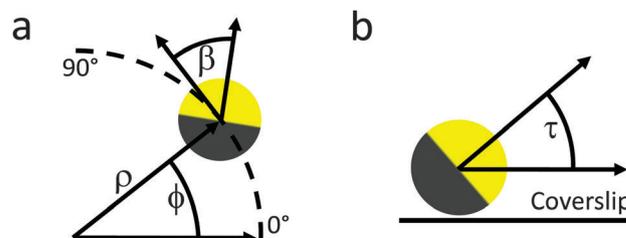$$A = \frac{kD}{2\pi k_B T},\qquad(3)$$

Fig. 4 Plan (a) and side (b) views of a Janus swimmer orbiting a colloid, showing the definition of the angles ϕ, β and τ, and the orbital radius ρ. The mean values of β and τ are $\langle \beta \rangle = 7° \pm 2°$, and $\langle \tau \rangle = 1° \pm 2°$.

where k has the dimensions of stiffness and D is a relevant diffusivity. In our case, the simplest escape routes come from large fluctuations in β or ρ. For fluctuations in ρ, we estimate $k = k_\rho$. To estimate the relevant D, we have to know the effect of nearby surfaces on diffusion normal to these surfaces. It is known that for a surface-to-surface gap of $g = 0.1a$ (we measured gaps of this order; see Appendix B), the diffusivity D_ρ for a swimmer close to a single plane wall is approximately 10% of the free-particle diffusivity,[43] giving $D_\rho \sim 0.02$ μm^2 s^{-1} here. Using these values, we find $A_\rho \sim 30$ s^{-1}, which, together with $\Gamma = 10^{-3}$ s^{-1} at 10% H_2O_2, gives $U \sim 12k_BT$. Considering fluctuations in β gives a similar result.

Note that in the above σ_β and σ_ρ are averages of the standard deviations obtained from single orbits, rather than orbit-to-orbit variations. We found no oscillations in these parameters,‡ so that the measured standard deviations represent a combination of real temporal variabilites in these parameters and experimental uncertainties in their measurement. In consequence, k_β, k_ρ and U represent approximate lower bounds on the respective quantities.

Finally, we point out that our findings should also apply generally to the trapping of Janus swimmers at surfaces and edges, since the orbital trapping appears to be a particular instance of this more general case. As previously noted,[7] micron-sized catalytic Janus swimmers are stably trapped at glass surfaces, and we have also observed their trapping on the surfaces of 100 μm polystyrene beads (Thermo Scientific), and of hexadecane (Sigma Aldrich) droplets. The orbital behaviour found here also appears to be generic: we have observed stable orbits around silica beads (Bangs Labs), hexadecane droplets, and the oxygen bubbles formed by the H_2O_2 decomposition.§ The swimmers also follow the internal edge of water droplets on glass in air or in oil, and will orbit around the horizontal axis between two colloids within the colloidal crystals if a defect leaves sufficient space.¶ Orbital behaviour has also been reported for Pt–Au nanorods,[32] and again, this was with static colloids of various materials.

2.3 Speed oscillations

In 10% H_2O_2, the orbits are extremely stable, and we tracked Janus swimmers orbiting single colloids within the crystal for 100s of revolutions (see ESI,† Video S2). The speed $u(\phi)$ as a function of the orbital angle ϕ shows sinusoidal oscillations (Fig. 5a). The solid curve is a fit of the form

---

‡ The reason for the lack of oscillation in β and ρ, as compared to the orbital speed (see below), is simply that β and ρ are constrained by the orbital trapping, whereas ϕ is not.

§ These oxygen bubbles can be a serious issue for experiments on self-propelled particles fuelled by H_2O_2. The relatively low concentration of Janus particles used here allows us to make measurements for at least 1 hour before these bubbles intrude significantly on the swimming experiments. However, the oxygen bubbles did limit electrophoretic mobility measurements to a maximum of 1% H_2O_2 (see Appendix C).

¶ In a perfectly hexagonally ordered layer of 10 μm diameter spheres, the interstice between three neighbouring spheres is too small for the passage of a 2 μm diameter sphere.
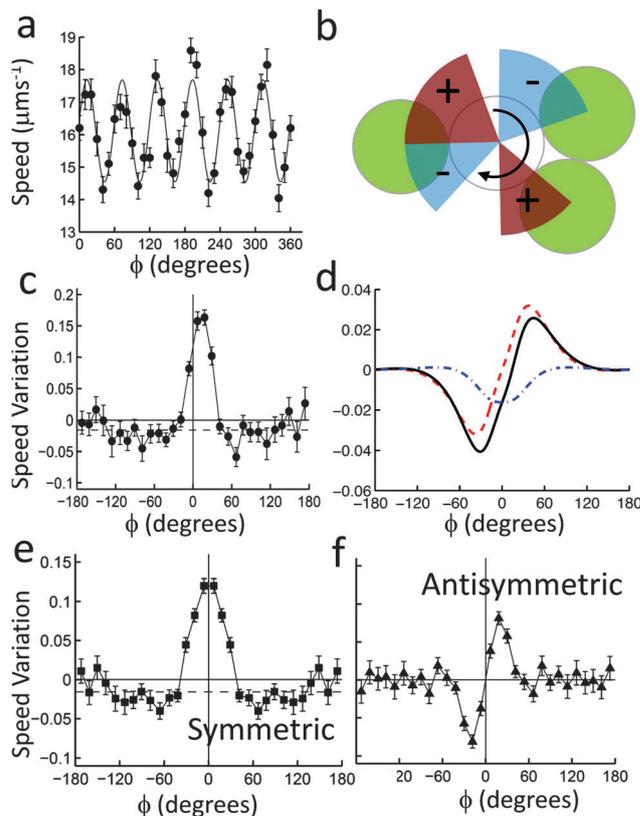

Fig. 5 (a) Typical oscillations in orbital speed, from ~200 revolutions of a Janus swimmer inside a crystal, in 10% H_2O_2. Solid curve: 60° Fourier component. (b) Cartoon illustrating the reconstruction of the speed variation on passing near a single neighbouring colloid. For a clockwise orbit, points in the red regions are assigned $\phi > 0$, and the blue regions $\phi < 0$, with $\phi = 0$ at the contact point between the central colloid and each respective neighbour. The uncoloured regions are not included, as they are within 90° of two neighbouring colloids. (c) Reconstructed, fractional speed variation caused by orbiting past a single neighbouring colloid at $\phi = 0°$, averaged over 35 swimmers. Dashed, horizontal lines indicate the average speed outside the perturbed region, $-90° < \phi < 90°$. (d) Theoretical fractional speed variation (black, solid) of a pusher with stresslet amplitude $\alpha = 1$ swimming past a neighbouring colloid, as described in the text. The antisymmetric (red, dashed) and symmetric (blue, dot-dashed) components are also shown. (e) Symmetric, and (f) antisymmetric parts of the speed variation in c.

$$u(\phi) = u_c\{1 + \tilde{u}\cos[6(\phi - \delta)]\}, \qquad (4)$$

with $\delta \in (-30°, 30°)$. The origin for ϕ is chosen so that the neighbouring colloids are at $\phi = 0°$, 60°, etc. We measure from 17 videos a fractional amplitude $\tilde{u} = 7.7\% \pm 0.5\%$ and retardation $\delta = 13.5° \pm 1.5°$. It is clear that these oscillations originate from interactions between the Janus swimmer and the six colloids neighbouring the central colloid. However, there are several possible types of interaction, which we will now discuss.

As before, we begin with passive interactions. The surface-to-surface distance between the Janus swimmer and its neighbouring colloids is at least 800 nm, so, again, the only plausible passive interaction mechanism is electrostatic. Adding 100 μM

NaNO$_3$ (giving Debye length, $\kappa^{-1} \lesssim 30$ nm) left the oscillations unchanged, and in this case we can estimate the minimum charge density q needed to give the observed oscillation amplitude. The screened potential between two charged spheres is

$$U = \frac{4\pi q^2 aR}{\varepsilon\kappa^2(g + a + R)}\exp(-\kappa g), \qquad (5)$$

where g is the surface–surface separation and ε is the dielectric permittivity of water.[44] The maximum amplitude is therefore

$$\delta u_{max} \approx \frac{1}{6\pi\eta a}\left|\frac{\partial U}{\partial g}\right|. \qquad (6)$$

The observed amplitude of $\delta u \sim 1$ μm s^{-1} requires an unrealistically high charge density of $q \gtrsim 1$ C m^{-2}, approximately 1000 times our measured values of $\sim 10^{-3}$ C m^{-2} (Appendix C). Therefore, passive electrostatic interactions cannot generate the observed speed oscillations.

In principle, the oscillations could be due to spatial variations in absolute H$_2$O$_2$ concentration directly affecting the swimming speed. However, the propulsion speed is insensitive to H$_2$O$_2$ concentration at 10% H$_2$O$_2$ (Fig. 3a). Furthermore, the measured H$_2$O$_2$ consumption rate[7] implies that these swimmers will deplete the H$_2$O$_2$ concentration at their surface by only around 1% of the bulk concentration. Therefore, these local variations in fuel concentration cannot account for the observed speed oscillations.

We therefore turn again to active interactions. First, however, we note that the geometry within the crystal is extremely confined, and that it would be simpler to consider the interaction between an orbiting swimmer and a single neighbouring colloid. We were not able to obtain isolated pairs of colloids, so we instead measured $u(\phi)$ for swimmers orbiting colloids at the edge of the crystal, having between 2 and 4 neighbours. For each swimmer, we analyse only those parts of its orbit where the swimmer does not have more than one neighbouring colloid within a $\pm 90°$ sector (see Fig. 5b). These partial trajectories are then averaged together to reconstruct the effect of a single neighbour.

The reconstructed $u(\phi)$ is shown in Fig. 5c. A single peak is seen just after the swimmer passes a neighbour. The speed variation is practically nil by $\phi = 60°$, *i.e.*, a swimmer is little affected by colloids beyond the one or two neighbouring colloids nearest to it. In fact, if we add together six suitably shifted copies of the data in Fig. 5c, we obtain an oscillation whose 60°-period sinusoidal component has amplitude 7% and retardation 13°, consistent with the experiments performed inside the crystal.

Even with this simplification of the geometry, interpreting these oscillations further is problematic without detailed knowledge of the propulsion mechanism. This is because of the presence of both hydrodynamic and phoretic fields. Even where the phoretic fields are electrostatic, they may be long-ranged, since they involve ionic currents, and are therefore not subject to the equilibrium ionic screening. Furthermore, phoretic fields generate interactions in two ways: (i) by direct reflection from discontinuities, here the liquid–static-colloid interfaces; and (ii) by generating osmotic flows through coupling to any finite mobility of those interfaces, *i.e.* the charged surfaces of the static colloids.

Due to these complications, we neglect PI here and discuss the speed variations expected for a model swimmer in our geometry subject only to HI, comparing these predictions to our experiments. Understanding the role of hydrodynamics should, of course, contribute to a future full theory that also involves PI.

We use the lowest-order model for the flow field **u** around a force-free swimmer, which is a stresslet (force dipole) field **S** of amplitude α. So, **u** = α**S** with, in spherical polars,

$$\mathbf{S} = \frac{1}{2r^2}(1 + 3\cos 2\theta)\hat{\mathbf{r}}, \qquad (7)$$

where θ is the angle from the swimmer's unperturbed propulsion direction and $r\hat{\mathbf{r}}$ is the vector displacement from its center. Different types of swimmers are distinguished by the symmetry of their surrounding flow fields, *i.e.* the sign of the prefactor α (Fig. 6a). Pushers (*e.g. E. coli*) have amplitude $\alpha > 0$, while pullers (*e.g.* various *Chlamydomonas* algae) have $\alpha < 0$. In neutral swimmers, $\alpha = 0$, and higher order terms become important.

In Fig. 5e–f, we split the observed speed variation up into antisymmetric and symmetric parts around the point where a swimmer passes a neighbouring colloid. Comparison of Fig. 6b with Fig. 5f shows that our observations are consistent with a pusher. As a pusher approaches the neighbouring colloid, the fluid pushed out in front is reflected by the colloid and slows the swimmer down; once the swimmer has passed the colloid, the fluid pushed out behind speeds it up.

If this speed variation is solely due to the stresslet component, we can estimate α by calculating the approximate hydrodynamic interaction between a free stresslet swimmer in circular orbit and a spherical surface (the neighbouring colloid) outside that orbit. We use the measured mean position and orientation of the swimmer with respect to the central colloid (see Appendix B), and a far-field analytical expression for the interaction of a stresslet with a spherical surface.[45] Calculation details are in Appendix D.
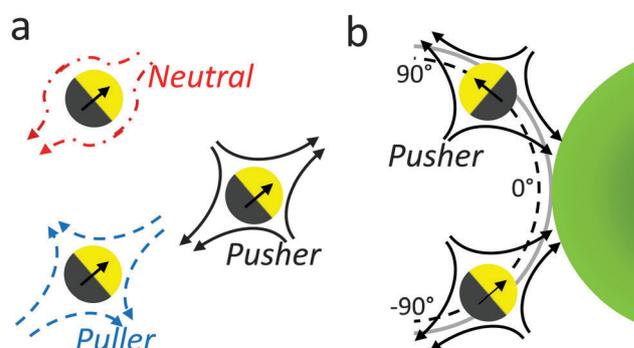

Fig. 6 (a) Schematics of the flow-fields around neutral, pusher and puller swimmers, in the lab frame. (b) Plan view of a pusher orbiting (dashed line) a central colloid (grey outline) with one neighbouring colloid (solid green).
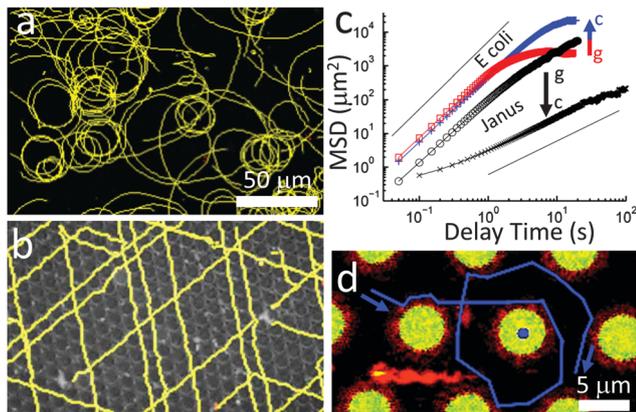
Fig. 7 Tracked videos of smooth-swimming *E. coli* (a) on plain glass, and (b) inside a crystal. (c) MSD on plain glass ($\bigcirc$ = Janus; $\square$ = *E. coli*) and inside the crystal ($\times$ = Janus, $+$ = *E. coli*). Solid lines: diffusive (t) and ballistic (t^2) scaling. Arrows highlight the effect of moving from glass into the crystal (g $\rightarrow$ c). (d) Confocal image of a flagella-stained (red) bacterium inside a colloidal crystal. Colloids (green) touch each other, but only a small, polar slice is visible. Blue: 6 s trajectory of a bacterium with shorter flagella (not shown).

Fig. 5d shows the predicted fractional speed variation $\Delta u/u_0$ for $\alpha = u_0 a^2$ (black solid), and the antisymmetric (red dashed) and symmetric (blue dot-dashed) components of this variation. The predicted speed variation would be completely antisymmetric for a swimmer oriented tangent to the orbit, but the inclination of the swimmer away from the orbit breaks this symmetry slightly. To match the peak heights between Fig. 5d and f requires $\alpha \sim 30\ \mu m^3\ s^{-1}$. This appears reasonable, as *E. coli* of a similar size moving at a similar speed have a measured $\alpha = 40\ \mu m^3\ s^{-1}$.[24] Nevertheless, our value is no more than a very rough estimate. Moreover, the stresslet contribution clearly cannot fully explain the observed speed oscillations. Further analysis of the HI, including interaction with the central colloid and the plane surface, as well as future advances enabling the inclusion of PI, will be necessary before firm conclusions can be drawn.

3 *E. coli* bacteria

3.1 Materials and methods

Motile, GFP-labelled smooth-swimming *E. coli* (strain AB1157 $\Delta cheY$), were cultured as previously described[16,46] and suspended in motility buffer (see Appendix E for details) before being loaded into chambers with or without colloidal crystals. Further genetic modification permits tight binding of a fluorescent dye (Alexa Fluor 633) to the flagella bundle (see Appendix E for details). The flagella-labelled GFP-expressing *E. coli* were observed in a Zeiss confocal microscope at 4 fps using laser excitation at 488 nm (for GFP) and 633 nm (for Alexa Fluor 633). We added 0.2 wt% TWEEN 20 to minimise adhesion of bacteria to the glass.[16]

3.2 Rectification of trajectories

Fig. 7a and b shows trajectories of *E. coli* bacteria outside and inside a colloidal crystal. On plain glass, these bacteria circulate

clockwise (viewed from the fluid side) due to their rotating flagella.[33–35] The crystal rectifies this circulation into straight trajectories. Fig. 7c shows the MSD of *E. coli* averaged over 5 videos per curve. Outside the crystal, trajectories are initially ballistic, levelling off at long times due to the circular motion. Inside the crystal, the ballistic regime is extended, because the bacteria cannot circulate. For comparison, we also show the MSD of Janus particles in 1% H_2O_2. Here, the effect on the MSD is reversed: on plain glass, the Janus swimmers move ballistically (MSD $\propto \Delta t^2$, with Δt = delay time) at short times, becoming diffusive (MSD $\propto \Delta t$) at long times due to rotational diffusion,[5] whereas in the crystal, they are diffusive at all times longer than the orbital time.

The behaviour of *E. coli* can be explained more simply than that of the Janus swimmers. The bacteria's typical circulation radius (Fig. 7a) is much larger than the inter-colloid spacing, and at $\sim$7 μm, their flagella are likely to hinder turning out of the straight channels between colloids. Occasionally, bacteria do briefly orbit individual colloids, but imaging *E. coli* with fluorescent flagella, shows that these cells typically have shorter, $\sim$3 μm flagella (Fig. 7d and ESI,† Video S3), and so should also have a naturally tighter circulation radius than bacteria with longer flagella.[34] Unlike Janus swimmers, bacteria do not appear to be trapped by the colloid at the centre of their orbit, and do not approach it closely (Fig. 7d). This is consistent with recent experiments on the orbital trapping of *E. coli* by microfluidic posts:[31] significant trapping was observed only for posts of greater than 50 μm radius.

It is interesting that the complex environment of the colloidal crystal can effectively simplify the trajectories of *E. coli* bacteria compared to their behaviour on plane surfaces. This may have applications in studying various-taxes (chemotaxis, phototaxis *etc.*) on surfaces, where circulation would normally prevent the bacteria from biasing their motion along favourable gradients.

4 Conclusion

We have studied the behaviour of catalytic Janus swimmers and motile *E. coli* bacteria inside a model 2D colloidal crystal. The effect of this porous environment on these two swimmers is, respectively, to create and destroy, orbital motion.

Our measurement of the behaviour of Janus swimmers inside the colloid crystal has generated a wealth of data on their behaviour in this environment, including detailed characterisation of orbital speed oscillations. These data set constraints for future work on the propulsion mechanism of these swimmers. Such understanding would then allow an assessment of the importance of PI in our crystalline geometry. If PI turn out to be minor, then our analysis of HI suggests that Janus swimmers are pushers with similar dipolar flow field amplitude to *E. coli*. In that case, the very different response to the crystalline environment of these two self-propelled particle systems is noteworthy: many theoretical calculations and simulations assume, at least implicitly, that it is fruitful to discuss 'generic pusher behaviour'. Our data suggest otherwise.

Our observations immediately suggest other studies. For example, the circulation of *E. coli* next to surfaces presents an obstacle to the study of chemotaxis, which crystalline rectification would presumably overcome. The stable Janus swimmer orbits at high fuel concentration could form the basis for constructing various microfluidic devices, *e.g.*, a mixer on the micro level.[32]

Appendix

A Supplementary video information

SV1 – Janus swimmers moving through a colloidal crystal in 1% H_2O_2. Epifluorescence, at 3 fps, 50 μm scale bar.

SV2 – High magnification video of a Janus swimmer orbiting a single colloid inside a crystal in 10% H_2O_2. Epifluorescence (initially brightfield to show location of neighbouring colloids) at 20 fps, 5 μm scale bar.

SV3 – Confocal video of *E. coli* bacteria with green stained bodies and red stained flagella swimming inside a colloidal crystal (green). The colloids touch each other, but only the poles are visible. Early in the video, an *E. coli* with short flagella orbits the colloid marked with a blue circle. 4 fps, 10 μm scale bar.

SV4 – High magnification, edge-on video of a Janus swimmer orbiting a single colloid at the edge of a crystal in 10% H_2O_2. Epifluorescence at 20 fps, 5 μm scale bar.

B Geometrical considerations

In this section, we give details of how we estimate the gap sizes and inclination angles between the surface of the swimmer, and the static colloid and glass surfaces.

As the swimmer orbits a single colloid, we wish to measure the radius ρ of its orbit, the azimuthal angle of the swimmer around its orbit ϕ, and the inclination β and τ of the swimmer's orientation away from the tangent to that orbit (see Fig. 4b). However, since the Janus particle has non-uniform fluorescence intensity, we cannot straightforwardly determine the centre of the particle. We instead measure equivalent parameters (ρ', ϕ', β') for the centroid of an ellipse fitted to a thresholded image of the swimmer at each frame, which will be offset from the true centre of the swimmer by some small distance Δc along the swimmer's orientation vector.

The expected shape of the image of the swimmer is not clear, since the Pt coating appears to only partially block out the underlying fluorescence (see ESI,† Video SV2). We estimate Δc from the aspect ratio of the fitted ellipse by performing identical ellipse fitting in MATLAB on two models of the changing thresholded shape of the swimmer, which take the lower half of the image to be either a half-ellipse or a truncated semicircle (Fig. 8a).

We plot the relationship between the difference ΔL in the fitted major and minor axis lengths, and the offset of the centroid Δc in these two models, and use the average of these two curves to estimate the experimental value of Δc. The radius of the Janus swimmers is $a = 0.96 \pm 0.04$ μm, and, averaging over 17 videos, we find $\Delta L = 360 \pm 20$ nm, giving $\Delta c = 135 \pm 30$ nm, where the
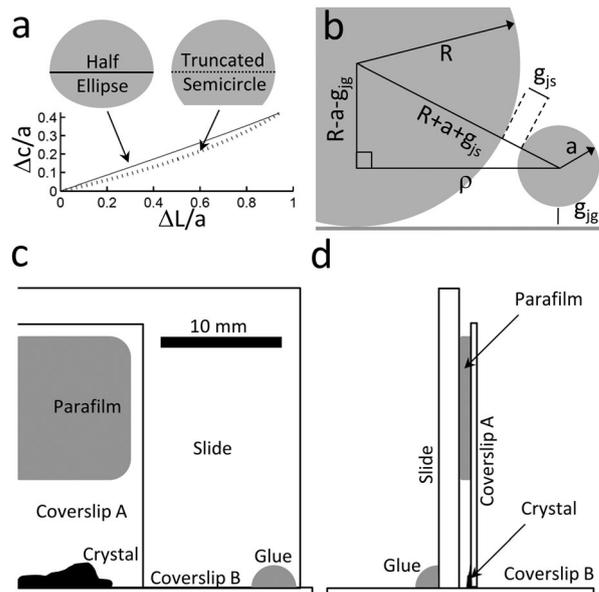

Fig. 8 (a) Results of estimating the offset of a fitted ellipse $\Delta c/a$ from the difference in fitted axis lengths $\Delta L/a$ based on two models shown here and described in the text. (b) Side view of a swimmer orbiting a colloid (not to scale) with geometrical construction to determine the size of the gaps g_{js} and g_{jg} between the swimmer and the colloid or plane. (c and d) Diagrams of the sample cell for observation along the plane of the coverslip. Observation is from below coverslip B, through the crystal and along the plane of coverslip A. Diagram (c) has been cut in half along the left edge of the figure.

difference between the two curves in Fig. 8a has been taken into account in the uncertainty. To lowest order in Δc, the corrections to ρ, ϕ and β are then given by

$$\rho = \rho' - \Delta c \langle \sin \beta' \rangle,$$
$$\phi = \phi' - \frac{\Delta c}{\langle \rho' \rangle} \langle \cos \beta' \rangle, \qquad (8)$$
$$\beta = \beta' - \frac{\Delta c}{\langle \rho' \rangle} \langle \cos \beta' \rangle.$$

The corrections are approximately 20 nm, and $2°$ respectively, and these have already been applied here and in the body of the article, to give $\langle \rho \rangle = 4.56 \pm 0.02$ μm and $\langle \beta \rangle = 7° \pm 2°$.

From the average value of the orbital radius $\langle \rho \rangle$, we calculate the size of the gaps between the swimmer surface and the static colloid g_{js} or the plane glass surface g_{jg}. The geometric construction in Fig. 8b gives the following expression for g_{js} and g_{jg}

$$\rho^2 + (R - g_{jg} - a)^2 = (R + g_{js} + a)^2, \qquad (9)$$

where the radius of the static colloids, $R = 5.06 \pm 0.02$ μm, and the averages $\langle \cdots \rangle$ have been dropped for convenience. This single equation cannot be used to solve for both g_{js} and g_{jg}. However, since both gap sizes must be positive, we can obtain upper bounds on each

$$g_{jg} < \frac{\rho^2 - 4Ra}{2(R - a)},$$
$$g_{js} < \frac{\rho^2 - 4Ra}{2(R + a)}, \qquad (10)$$

where we have ignored small terms quadratic in g_{jg}, g_{js}. Calculating these limits gives $g_{js} < 200$ nm and $g_{jg} < 300$ nm, taking the largest value within experimental error. If instead, we assume that $g_{jg} = g_{js} = g$, eqn (9) gives

$$g = \frac{\rho^2}{4R} - a = 70 \pm 10 \text{ nm}. \tag{11}$$

For an order-of-magnitude consistency check on this value, we obtained the translational diffusivity D_c of the swimmers within each orbit from the ballistic component of the angular MSD $\langle (\phi(t) - \phi(0))^2 \rangle$, obtaining $D_c = 0.082 \pm 0.006$ μm^2 s^{-1}, independent of the swimming speed. We note that D_c, is a factor of ~ 3 smaller than the predicted Stokes–Einstein bulk diffusivity $D_{SE} = k_B T / (6\pi \eta a) = 0.23$ μm^2 s^{-1} in the bulk. Proximity to walls generally decreases the translational diffusivity of particles.[47] Our geometry is rather complex, and, to our knowledge, has not been treated theoretically. However, since the swimmer is close to two surfaces, and cannot rotate, we may expect a reduction in diffusivity similar to that for a particle moving in the central plane between two parallel plates. Experiments have been performed measuring the drag on spheres moving axially along the centre line of rectangular prisms of aspect ratios $10:1$, and these also find a correction factor ≈ 3 for $g/a = 0.1$,[48] where g is the gap width. Eqn (11) gives $g/a \sim 0.07$ in our case, so that the similarity in the diffusivity reduction factors is reassuring.∥

To obtain the inclination τ w.r.t. the glass plane, 10 Janus swimmers orbiting colloids in the crystal were observed along the plane of the coverslip using a custom-built sample chamber, shown in Fig. 8c and d. A colloidal crystal was formed at the edge of a 22×22 mm² coverslip (A), as in the main text. Coverslip A was attached with ~ 600 μm parafilm to a glass slide previously cut down to 50 mm, so that the edge of coverslip A was flush with the long edge of the slide, with the crystal facing inwards. The slide was then glued onto a 22×50 mm² coverslip (B), with the crystal lying next to coverslip B. Janus swimmers in 10% H_2O_2 solution were added as usual, and viewed through coverslip B using a $100\times$ oil immersion objective. Swimmers were recorded orbiting single colloids at the lower edge of the crystal, and images were captured with a CoolSNAP (Photometrics) camera using MicroManager[49] (see ESI,† Video S4). The inclination $\tau = 1° \pm 2°$ of the swimmers w.r.t. coverslip A was determined by fitting ellipses to thresholded images of the swimmers, as above.

C Electrophoretic mobility measurements

We used a Malvern Zetasizer to measure the electrophoretic mobility of each of the colloids, in a solution of 100 μM $NaNO_3$ (Fluka) and 1% H_2O_2. The colloidal volume fractions were 10^{-5} v/v for all 2 μm diameter colloids, and 10^{-3} v/v for all 10 μm diameter colloids.

The mobilities were, for the 2 μm diameter, uncoated polystyrene colloids, $\mu_{PS} = (-4.7 \pm 0.2) \times 10^{-8}$ m² V⁻¹ s⁻¹,

---

∥ We also measured the diffusivity on plain glass, $D_g = 0.21 \pm 0.01$ μm^2 s⁻¹ independent of H_2O_2 concentration, in agreement with previous measurements.[5,7,8] This is similar to the Stokes-Einstein prediction. However, without a precise measurement of the bulk diffusivity or viscosity, we cannot use this measurement to estimate the swimmer-glass-surface gap.

and for the Janus particles $\mu_j = (-4.1 \pm 0.6) \times 10^{-8}$ m² V⁻¹ s⁻¹. The mobility of a half-coated Janus particle should just be the mean mobility of its faces,[50] which implies a Pt surface mobility of $\mu_{Pt} = (-3.5 \pm 1.2) \times 10^{-8}$ m² V⁻¹ s⁻¹. For the static colloids, $\mu_S = (-3.2 \pm 0.2) \times 10^{-8}$ m² V⁻¹ s⁻¹.

Applying the Smoluchowski theory for the electrophoretic mobility, the surface charge density on these colloids is approximately $q = \mu \eta \kappa$, with $\kappa^{-1} \sim 30$ nm the Debye length, and $\eta = 10^{-3}$ Pa s the viscosity of water, giving q of order (-10^{-3}) C m⁻² in each case.

We were unable to measure Janus particle mobilities in 10% H_2O_2, because the production of oxygen bubbles interfered with the measurement. However, we verified that Janus particles in 1% H_2O_2 with 100 μm $NaNO_3$ exhibit the same orbital trapping behaviour.

D Hydrodynamic interactions

In this section, we write down, for a swimmer moving in a circular orbit in free space, the speed variation induced by hydrodynamic interaction with a spherical object outside that orbit. The swimmer is modelled as a stresslet of strength α, oriented along a swimming direction $\hat{\mathbf{v}}$. The swimmer is instantaneously located at position $\mathbf{s}$, lying on a circular orbit whose local tangent vector is $\hat{\mathbf{p}}$. A colloid of radius R is located at some arbitrary position $\mathbf{X}$. The displacement vector $\mathbf{l}$ of the swimmer from the static colloid is $\mathbf{l} = \mathbf{s} - \mathbf{X}$, with center-to-centre distance $l = |\mathbf{l}|$. The distance between the centre of the swimmer and the surface of the neighbouring colloid is $h = l - R$.

We decompose the swimmer's orientation into components perpendicular and parallel to the neighbouring colloid's surface, in order to use the expressions for the advected velocity given in Spagnolie et al.[45] We therefore define two unit vectors, $\hat{\mathbf{l}}$, which is perpendicular to the colloid surface, and $\hat{\mathbf{k}}$ which is parallel to the colloid surface, and lies in the $\hat{\mathbf{v}}$, $\hat{\mathbf{l}}$ plane. These two unit vectors are

$$\hat{\mathbf{l}} = \frac{\mathbf{l}}{l},$$
$$\hat{\mathbf{k}} = \frac{\hat{\mathbf{l}} \times (\hat{\mathbf{v}} \times \hat{\mathbf{l}})}{|\hat{\mathbf{v}} \times \hat{\mathbf{l}}|}. \tag{12}$$

In this coordinate system

$$\hat{\mathbf{v}} = \hat{\mathbf{k}} \cos \omega + \hat{\mathbf{l}} \sin \omega, \tag{13}$$

where ω is the inclination of the swimmer away from the tangent plane to the colloid's surface ($\sin \omega = \hat{\mathbf{v}} \cdot \hat{\mathbf{l}}$). We can define two other angles likewise: $\sin \psi = \hat{\mathbf{p}} \cdot \hat{\mathbf{l}}$, and $\cos \chi = \hat{\mathbf{p}} \cdot \hat{\mathbf{v}}$.

The hydrodynamic interactions between a free swimmer, moving originally at speed u_0 along direction $\hat{\mathbf{v}}$, and the sphere, would in general result in an additional swimmer velocity $\Delta \mathbf{u}$, which can be decomposed along $\hat{\mathbf{l}}$ and $\hat{\mathbf{k}}$

$$\Delta \mathbf{u} = u_l(h, \omega, u_0) \hat{\mathbf{l}} + u_k(h, \omega, u_0) \hat{\mathbf{k}}. \tag{14}$$

In the present case, however, the particle velocity is constrained to lie on the tangent, $\hat{\mathbf{p}}$, so the observed variation in swimmer

speed will be $u' = \hat{\mathbf{p}} \cdot \Delta\mathbf{u}$, or

$$u' = u_l \sin\psi + u_k \frac{\cos\chi - \sin\psi\sin\omega}{\cos\omega}, \qquad (15)$$

where, for the velocity components u_l and u_k, we can directly use recently derived far-field interaction formulae.[45] Translating into our coordinate system, these are

$$u_l = \frac{-3R\alpha(1 - 3\sin^2\omega)(R + h)}{2h^2(2R + h)^2}$$

$$u_k = \frac{3R^3\alpha(2R^2 + 6Rh + 3h^2)\sin(2\omega)}{4h^2(R + h)^3(2R + h)^2}. \qquad (16)$$

and combining eqn (15) and (16) will then give the predicted fractional speed variation u'/u_0.

It remains to write down the relevant coordinates. The (fictitious) glass surface is on the x–y plane, with z pointing into the sample, and the origin is at the point of contact between the (fictitious) central colloid and the plane. We take the swimmer to be a small distance $g_{jg} = 70$ nm above the plane, and orbiting at horizontal distance ρ from the z-axis through the centre of the central colloid ($x = y = 0$), and define its position $\mathbf{s}$ in terms of the azimuthal angle ϕ

$$\mathbf{s} = (\rho\cos\phi, \quad \rho\sin\phi, \quad a + g_{jg}). \qquad (17)$$

The neighbouring colloid is fixed at

$$\mathbf{X} = (2R, \quad 0, \quad R), \qquad (18)$$

while the tangent to the circular orbit of the swimmer is

$$\hat{\mathbf{p}} = (-\sin\phi, \quad \cos\phi, \quad 0), \qquad (19)$$

and the orientation of the swimmer is

$$\hat{\mathbf{v}} = (-\sin(\phi - \beta)\cos\tau, \quad \cos(\phi - \beta)\cos\tau, \quad \sin\tau), \qquad (20)$$

where β is the fixed angle between the tangent to the orbit and the orientation of the swimmer in the x–y plane, and τ is the fixed inclination of the swimmer away from the horizontal plane (Fig. 4). This gives $\cos\chi = \cos\beta\cos\tau$.

E Flagella stained *E. coli*

Construction of the smooth swimming *E. coli* strain AB1157 *che*Y has been described previously.[46] For the current work, the strain was further modified by replacement of the chromosomal copy of the *fli*C gene with a modified copy encoding a mutant FliC protein in which the serine amino acid at position 353 is replaced with a cysteine amino acid. Strain HCB1668 is a Tn5 *fli*C null derivative of AW405 in which FliC S353C is expressed from the plasmid pBAD33.[51] This plasmid was used as a template to amplify 803 bp of *fli*C by PCR. This encompassed the AGT to TGC mutation which was flanked on each side by 400 bp of the *fli*C gene. The primers used for amplification were GCAACTCGAGCAATTGAGGGTGTTTATACTGA and GCAAGTCGACCCTGGTTAGCTTTTGCCAACA. Restriction sites for XhoI and SalI were included. The PCR product was purified, digested with XhoI and SalI and ligated into the plasmid pTOF24,

which had been digested with the same enzymes. The resultant recombinant plasmid pTOF24 *fli*C was transformed into AB1157 *che*Y and used to replace the wild type *fli*C allele with the *fli*C mutation by plasmid mediated gene replacement using a previously published method.[52] Correct insertion of the mutation was verified by sequencing.

The resultant strain AB1157 *che*Y pHC60 FliC S353C was grown from a single colony in 10 ml Luria-Bertani broth containing 30 μg ml^{-1} kanamycin and 5 μg ml^{-1} tetracycline overnight at 30 C and 200 rpm. Bacteria were diluted 1 : 100 into 35 ml tryptone broth containing antibiotics as above and grown for a further 4 h. Next, three washes were performed using phosphate motility buffer (6.2 mM K_2HPO_4, 3.8 mM KH_2PO_4, 67 mM NaCl, 0.1 mM EDTA at pH 7.0) and the cells were concentrated to a total volume of $\sim$3 ml. To perform flagella labelling the protocol of Turner *et al.*[51] was followed. Briefly, 10 μl of Alexa Fluor 633 C5 maleimide (1 mg ml^{-1} in dimethyl sulfoxide, Molecular Probes) was added to 1 ml of washed bacteria and incubated at room temperature and 100 rpm for 60 min. Three washes were performed as described above and the final cell density was adjusted to optical density 0.3 at 600 nm in motility buffer containing 0.002 wt% TWEEN 20.

Acknowledgements

References

1 W. C. K. Poon, in *Physics of Complex Colloids*, ed. C. Bechinger, F. Sciortino and P. Ziherl, Società Italiana di Fisica, Bologna, 2013, pp. 317–386(= arXiv:1306.4799).

2 S. J. Ebbens and J. R. Howse, *Soft Matter*, 2010, **6**, 726–738.

3 W. F. Paxton, K. C. Kistler, C. C. Olmeda, A. Sen, S. K. St. Angelo, Y. Cao, T. E. Mallouk, P. E. Lammert and V. H. Crespi, *J. Am. Chem. Soc.*, 2004, **126**, 13424.

4 J. G. Gibbs and Y.-P. Zhao, *Appl. Phys. Lett.*, 2009, **94**, 163104.

5 J. R. Howse, R. A. L. Jones, A. J. Ryan, T. Gough, R. Vafabakhsh and R. Golestanian, *Phys. Rev. Lett.*, 2007, **99**, 048102.

6 S. Ebbens, M.-H. Tu, J. R. Howse and R. Golestanian, *Phys. Rev. E: Stat., Nonlinear, Soft Matter Phys.*, 2012, **85**, 020401.

7 A. T. Brown and W. C. K. Poon, *Soft Matter*, 2014, **10**, 4016–4027.

8 S. Ebbens, D. A. Gregory, G. Dunderdale, J. R. Howse, Y. Ibrahim, T. B. Liverpool and R. Golestanian, *Europhys. Lett.*, 2014, **106**, 58003.

9 M. C. Marchetti, J. F. Joanny, S. Ramaswamy, T. B. Liverpool, J. Prost, M. Rao and R. A. Simha, *Rev. Mod. Phys.*, 2014, **85**, 1143.

10 G. Volpe, I. Buttinoni, D. Vogt, H.-J. Kümmerer and C. Bechinger, *Soft Matter*, 2011, **7**, 8810.

11 Y. Fily and M. C. Marchetti, *Phys. Rev. Lett.*, 2012, **108**, 235702.

12 J. Stenhammar, A. Tiribocchi, R. J. Allen, D. Marenduzzo and M. E. Cates, *Phys. Rev. Lett.*, 2013, **111**, 145702.

13 J. Dunkel, S. Heidenreich, K. Drescher, H. H. Wensink, M. Bär and R. E. Goldstein, *Phys. Rev. Lett.*, 2013, **110**, 228102.

14 Y. Hatwalne, S. Ramaswamy, M. Rao and R. A. Simha, *Phys. Rev. Lett.*, 2004, **92**, 118101.

15 A. Zöttl and H. Stark, *Phys. Rev. Lett.*, 2014, **112**, 118101.

16 J. Schwarz-Linek, J. Arlt, A. Jepson, A. Dawson, T. Vissers, D. Miroli, T. Pilizota, V. A. Martinez and W. C. K. Poon, *Colloids Surf., B*, 2015.

17 R. Soto and R. Golestanian, *Phys. Rev. Lett.*, 2014, **112**, 068301.

18 W. E. Uspal, M. N. Popescu, S. Dietrich and M. Tasinkevych, *Soft Matter*, 2015, **11**, 434–438.

19 T. Bickel, A. Majee and A. Würger, *Phys. Rev. E: Stat., Nonlinear, Soft Matter Phys.*, 2013, **88**, 012301.

20 F. Ginot, I. Theurkauff, D. Levis, C. Ybert, L. Bocquet, L. Berthier and C. Cottin-Bizonne, *Phys. Rev. X*, 2015, **5**, 011004.

21 I. Theurkauff, C. Cottin-Bizonne, J. Palacci, C. Ybert and L. Bocquet, *Phys. Rev. Lett.*, 2012, **108**, 268303.

22 Q. Liao, G. Subramanian, M. P. DeLisa, D. L. Koch and M. Wu, *Phys. Fluids*, 2007, **19**, 061701.

23 K. Drescher, R. E. Goldstein, N. Michel, M. Polin and I. Tuval, *Phys. Rev. Lett.*, 2010, **105**, 168101.

24 K. Drescher, J. Dunkel, L. H. Cisneros, S. Ganguly and R. E. Goldstein, *Proc. Natl. Acad. Sci. U. S. A.*, 2011, **108**, 10940.

25 J. S. Guasto, K. A. Johnson and J. P. Gollub, *Phys. Rev. Lett.*, 2010, **105**, 168102.

26 T.-Y. Chiang and D. Velegol, *Langmuir*, 2014, **30**, 2600–2607.

27 K. Ishimoto and E. A. Gaffney, *Phys. Rev. E: Stat., Nonlinear, Soft Matter Phys.*, 2013, **88**, 062702.

28 G. Li and J. X. Tang, *Phys. Rev. Lett.*, 2009, **103**, 078101.

29 G.-J. Li and A. M. Ardekani, *Phys. Rev. E: Stat., Nonlinear, Soft Matter Phys.*, 2014, **90**, 013010.

30 G.-J. Li, A. Karimi and A. M. Ardekani, *Rheol. Acta*, 2014, **53**, 911–926.

31 O. Sipos, K. Nagy, R. Di Leonardo and P. Galajda, *Phys. Rev. Lett.*, 2015, **114**, 258104.

32 D. Takagi, J. Palacci, A. B. Braunschweig, M. J. Shelley and J. Zhang, *Soft Matter*, 2014, **10**, 1784.

33 M. A.-S. Vigeant, R. M. Ford, M. Wagner and L. K. Tamm, *Appl. Environ. Microbiol.*, 2002, **68**, 2794–2801.

34 E. Lauga, W. R. DiLuzio, G. M. Whitesides and H. A. Stone, *Biophys. J.*, 2006, **90**, 400–412.

35 H. Shum, E. A. Gaffney and D. J. Smith, *Proc. R. Soc. A*, 2010, **466**, 1725–1748.

36 J. Kotar, L. Debono, N. Bruot, S. Box, D. Phillips, S. Simpson, S. Hanna and P. Cicuta, *Phys. Rev. Lett.*, 2013, **111**, 228103.

37 A. I. Campbell and S. J. Ebbens, *Langmuir*, 2013, **29**, 14066.

38 J. C. Crocker and D. G. Grier, *J. Colloid Interface Sci.*, 1996, **179**, 298.

39 Y. Gu and D. Li, *J. Colloid Interface Sci.*, 2000, **226**, 328–339.

40 F. S. Lameiras, A. L. de Souza, V. A. R. de Melo, E. H. M. Nunes and I. D. Braga, *Mater. Res.*, 2008, **11**, 217–219.

41 J. Lintuvuori, A. T. Brown, K. Stratford and D. Marenduzzo, 2015, arXiv: 1508.04255.

42 P. Hänggi, P. Talkner and M. Borkovec, *Rev. Mod. Phys.*, 1990, **62**, 251.

43 R. G. Cox and H. Brenner, *Chem. Eng. Sci.*, 1967, **22**, 1753–1777.

44 M. Leunissen, C. Christova, A.-P. Hynninen, C. Royall, A. Campbell, A. Imhof, M. Dijkstra, R. Van Roij and A. Van Blaaderen, *Nature*, 2005, **437**, 235–240.

45 S. E. Spagnolie, G. R. Moreno-Flores, D. Bartolo and E. Lauga, *Soft Matter*, 2015, **11**, 3396–3411.

46 I. D. Vladescu, E. J. Marsden, J. Schwarz-Linek, V. A. Martinez, J. Arlt, A. N. Morozov, D. Marenduzzo, M. E. Cates and W. C. K. Poon, *Phys. Rev. Lett.*, 2014, **113**, 268101.

47 S. Kim and S. J. Karrila, *Microhydrodynamics: principles and selected applications*, Courier Dover Publications, 2013.

48 A. Miyamura, S. Iwasaki and T. Ishii, *Int. J. Multiphase Flow*, 1981, **7**, 41–46.

49 A. D. Edelstein, M. A. Tsuchida, N. Amodaj, H. Pinkard, R. D. Vale and N. Stuurman, *J. Biol. Methods*, 2014, **1**, e10.

50 J. L. Anderson, *J. Colloid Interface Sci.*, 1985, **105**, 45.

51 L. Turner, R. Zhang, N. C. Darnton and H. C. Berg, *J. Bacteriol.*, 2010, **192**, 3259.

52 C. Merlin, S. McAteer and M. Masters, *J. Bacteriol.*, 2002, **184**, 4573.

53 K. Schaar, A. Zöttl and H. Stark, *Phys. Rev. Lett.*, 2015, **115**, 038101.